Three-dimensional Change Detection and Description in Complex Construction Scenarios

Xuming Ge*, Xinjing Liu

Faculty of Geosciences and Engineering, Southwest Jiaotong University, 611756, Chengdu, China
xuming.ge@swjtu.edu.cn; liu_xinjing@my.swjtu.edu.cn

Keywords: Construction site, Laser point cloud, Change detection, Semantic description, Geometric change quantization.

Abstract

In large-scale engineering construction scenarios, construction objects and equipment are numerous; their spatial positions and postures change frequently and are complex and varied. Describing the changes between construction entities and the entities themselves in a three-dimensional (3D) geometric space and functional semantic space is challenging. In response to this challenging, we propose a novel workflow to detect and describe the changes in a construction site. First, we add the constraint of object surface continuity to the octree change detection (OCD), exclude the independently changing cells, and improve the change detection robustness. Second, based on the changes in entity elements that occur in the 3D geometric space, we introduce six-type semantics to characterize the changes that occur. Differing from existing change detection semantic description methods that focus on the attribute semantics of changed entity elements, our method focuses on the semantic description of the change process. Finally, for the variations in different semantic types, we propose specific quantization methods that can better quantify the variations in entity elements in 3D geometric space. For the proposed solution, we tested it using two sets of multi-period time-series point cloud data, which can accurately identify the changing construction entities in space and complete the calculation of bridge construction progress, including the building demolition and construction, and the change in the construction apparatus position.

1. Introduction

Perceiving changes in a construction scene is crucial for achieving progress detection, quality monitoring, and safety assurance in construction projects (Meyer et al.,2022). In large-scale construction projects, the extensive construction scene and numerous construction entities lead to complex and varied changes, rendering it difficult to accurately characterize the changes between construction entities and the entities themselves in three-dimensional (3D) geometric space and functional semantic space.

Compared to traditional two-dimensional (2D) change detection (Levine et al.,2023), three-dimensional change detection has real geographic coordinate and feature depth information. This enables the identification and updating of the posture of objects, real position changes, surface deformation and defects. Such capabilities satisfy the demand for 3D information in the construction process.

On one hand, advancements in LiDAR technology have significantly enhanced 3D change detection technology. On the other hand, the inherent limitations of laser point clouds, e.g., randomness, high noise levels, can pose challenges to change detection and description (Singh et al.,2023):

(1) Effective change is difficult to judge. In complex construction scenes, there is noise, imperfect data, and interference from natural changes, which render it easy to misjudge the change information.

(2) Locating the change object is difficult. Construction occurs over a long period and is multi-temporal; changes are widely distributed with complex processes, making it difficult to locate changes accurately.

(3) Difficulty in matching homonymous entity elements. Man-made construction objects are prone to structural symmetry and component occlusion, leading to difficulties in confirming the postures and positions of entity elements.

In order to address the aforementioned challenges and achieve more precise and efficient three-dimensional change detection and description in complex construction environments, scholars have conducted extensive research. This includes the relocalization methods (Duong et al., 2019), point cloud registration techniques (Li et al., 2020), utilization of octree technology (Park et al., 2021), and more to discover and describe spatial changes based on point clouds. Despite some progress in this task, there are still unresolved issues that require further refinement. In light of this, we designed a change detection framework for large and complex construction scenes. Our main contribution to this article is:

(1) Adding constraints on object surface continuity to octree change detection (OCD), reducing spatial occupancy change misjudgments, and improving 3D change detection robustness.

(2) Defining six types of semantics to semantically describe the change process and quantify the changes in construction entities, improving the cognitive power of these data.

(3) Proposing a stable alignment posture method for construction entity elements, obtaining the body orientation expression of the entity model, solving alignment problems caused by easily symmetric and structural occlusion of man-made objects.

2. Related works

2.1 Point-based change detection

In point-based change detection methods, changes are identified by calculating the difference in spatial location of either homonymous points or nearest neighbor points. Cloud2Cloud distance calculation method (Girardeau-Montaut et al., 2005) reflects point movements of two or more point-clouds at the same location generated from terrestrial laser scanning. In addition to point-to-point distances, changes can also be represented by point-to-surface or surface-to-surface distances. Distance-based differential estimation and occupancy grids can be mixed (Xiao et al., 2012) to detect changes in point clouds to improve the accuracy of variation calculation. Multiscale model-to-model cloud comparison distance measurements (Lague et al., 2013) can detect changes in complex terrain on point clouds without meshing. In addition, the variation calculation is less affected by the spatial point density, surface roughness and different

This contribution has been peer-reviewed. The double-blind peer-review was conducted on the basis of the full paper.
https://doi.org/10.5194/isprs-annals-X-4-2024-125-2024 | © Author(s) 2024. CC BY 4.0 License.

sampling positions. Height differences and gray-scale similarity of distances method (Du et al., 2016) are used to show building modifications based on existing information of the scene, in order to detect the change from observed distances.

Single-dimensional changes such as building height and terrain undulation can be computationally achieved by point-based change detection, but it is not possible to achieve posture monitoring and entity position change monitoring. To achieve change detection and chronological monitoring at construction sites, we need to combine other methods.

2.2 Voxel-based change detection

The voxel-based change detection method divides the point cloud into 3D grid cells or voxels. Changes are detected by comparing the occupancy status of a grid or voxel. However, the data characteristics of the point cloud create uncertainty in the visibility of the occupancy grids (Stilla et al, 2023). Occupancy grids with the Dempster–Shafer theory (Pagac et al., 1998) is used to establish and sustain environment maps for self-driving cars. Hebel et al. (2013) demonstrated variation as an occupancy grid. Occupancy analyses can be augmented with other metrics to estimate variance. For instance, Xiao et al. (2016) combined occupancy checks with point-to-triangle distances to assess point consistency in occupancy analyses, addressing variances in point densities and occlusions. Ray casting can lead to artifacts when traversing negative discrete spaces. Gehrung et al (2018) used planar knowledge to avoid such artifacts and later implemented octree to index changes, which improved change detection efficiency.

Voxel-based change detection is less impacted by point density compared with point-based change detection, resulting in improved efficiency, but it does not account for high-level semantic changes. We conducted semantic analyses of change objects utilizing voxel-based change detection to attain a dual enhancement in work efficiency and semantic clarity.

2.3 Object-based change detection

Object-based change detection can detect semantic label changes by using deep learning. Random Forest algorithm (Tran et al., 2018) trains artificial features on multi-targeted multi-temporal features, performs change detection and classification in a single step to avoid multi-step error transfer. Concatenated or feed-forward early fusion network on a 2.5D DSM (digital surface model) is used to acquire binary building classification changes (Zhang et al., 2019). Siam Graph Convolutional Network is used to define five change label types, performs change detection on 3D point clouds of complex street scenes (Ku et al., 2021). Convolutional operator (Landrieu et al., 2018) can also be used on segmentation change detection. Wang et al. (2018), introduced the underlying graph representation, which maps the initial point cloud onto the graph structure for semantic segmentation change detection. Siamese KPConv framework (de Gélis et al., 2023) is dedicated to change detection and classification of 3D point clouds, completes the extraction of six change types in urban scenes. However, the accuracy of this variation’s estimation is highly dependent on the classification or segmentation results.

The deep learning methods need enough amounts of labeled data to ensure classification accuracy. However, in construction scenes, the changing objects' structures are intricate, the high diversity and complexity of transformation types all contribute to an increase in the production cost of samples, subsequently reducing the model's generalization ability.

3. Methodology

3.1 Overview

We aim to attain effective and accurate change detection and quantitative analysis of complex construction scenes over time. The process is illustrated in Fig. 1. and involves optimized octree spatial change detection, spatial clustering segmentation of geometric changes objects, and measurement of change scales.

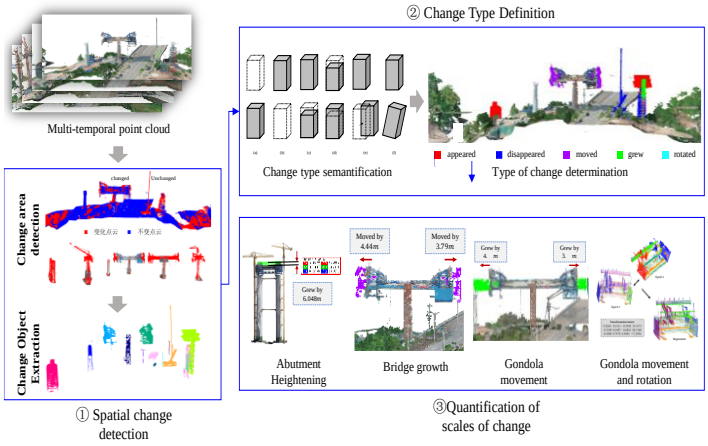

Figure 1. Workflow.

3.2 Robust octree spatial change detection

We aim to attain effective and accurate change detection and quantitative analysis of complex construction scenes over time. The process is illustrated in Fig. 1 and involves optimized octree spatial change detection, spatial clustering segmentation of geometric changes objects, and measurement of change scales.

We create an octree index with a change resolution of σm and add the next period of aligned point cloud data to the same octree. Spatially, the occupancy state can be represented by 0 and 1, that 0 is empty and 1 is occupied (Lu et al., 2019).

We define $U(a,b), a,b \in \{0,1\}$, as the space occupation state of the ontology, where a is the occupancy state of voxels in the first period, b is the occupancy state of voxels in the second period.

The change in the voxel occupied is:

$$C = \begin{cases} appeared, U = (0,1) \\ disappeared, U = (1,0) \\ unchanged, U \in \{(0,0)(1,1)\} \end{cases}. \quad (1)$$

We use Boolean operations (Mntyl, 1986) to search added nodes of the spatial octree and extract the geometric added point cloud under the added nodes.

We analyze the point cloud within voxels and the relationship between adjacent voxels to reduce the misclassification of interference point clouds.

The point distribution within a voxel can be classified into three cases: 1. isolated points within a voxel (See in Fig. 2(a)), 2. no common plane within a voxel (See in Fig. 2(b)), 3. finite planes within a voxel (See in Fig. 2(c)). Only in cases where the points within a voxel are finite planes are valid variations.

This contribution has been peer-reviewed. The double-blind peer-review was conducted on the basis of the full paper.
https://doi.org/10.5194/isprs-annals-X-4-2024-125-2024 | © Author(s) 2024. CC BY 4.0 License.

Change type	Semantics of change types	Mathematical description
appeared	The space occupied is empty at and occupied at .	$U(t_n) = 0\ and\ U(t\quad) = 1$
disappeared	The space occupied is occupied at and empty at .	$U(t_n) = 1\ and\ U(t\quad) = 0$
reduced	The volume changes, and it occupies more space at than at .	$V(U(t_n)) > V(U(t\quad))$
grew	The volume changes, and it occupies less space at than at .	$V(U(t_n)) < V(U(t\quad))$
moved	The volume and posture are unchanged, but its position changes between and t_{n+1}.	$V(U(t_n)) = V(U(t\quad))$, $L(U(t_n)) \neq L(U(t\quad))$
rotated	The volume and position are unchanged, but its posture changes between and t_{n+1}.	$V(U(t_n)) = V(U(t\quad))$, $L(U(t_n)) = L(U(t\quad))$, $A(U(t_n)) \neq A(U(t\quad))$

Table 1. Change type semanticization.

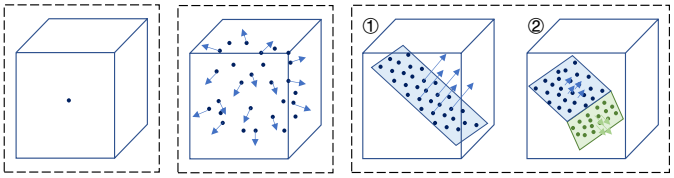

Figure 2. Normal vector distribution states of points within voxels. (a) Isolated points (b) Discrete distribution (c) points are distributed in planes: ①:one plane; ②: two planes.

When no neighboring voxels occur around a change voxel, the points within the voxel are outlier noise, which are considered invalid changes and are rejected.

First, changing voxels with a lot of point clouds smaller than the threshold are eliminated; we use the product of the octree resolution and the coefficient of the point cloud density as the threshold:

$$\varepsilon_x = a \cdot fm, (a < 1), \tag{2}$$

where ε_x is the judgment threshold, a is the product coefficient, f is the octree resolution, and m is the number of points per unit volume ($1\ m^3$) in the ideal case.

The voxel changes state at this point is:

$$C = \begin{cases} changed, \varepsilon \geq \varepsilon_x \\ unchanged, \varepsilon < \varepsilon_x \end{cases}. \tag{3}$$

Second, the normal direction of the points within the voxel is calculated, and those with the same normal direction are clustered, and the number of point cloud clusters —n is calculated.

At this point, the voxel changes state is:

$$C = \begin{cases} changed, n \neq \infty \\ unchanged, n = \infty \end{cases}. \tag{4}$$

Finally, the connectivity of the voxel is judged, and if neighboring voxels surround it, it is considered a valid change voxel.

At this point, the voxel changes state is:

$$C = \begin{cases} changed, k > 0 \\ unchanged, k = 0 \end{cases}, \tag{5}$$

where k is the current voxel’s number of neighboring voxels.

3.3 Semantic change process description

To express change types clearly and explicitly, we define the change types. We define the following six change types: appeared, disappeared, reduced, grew, moved, and rotated, as shown in Table 1, where $U(t_n)$ is the space occupancy state of the object, $V(U(t_n))$ is the space occupied volume of the object, $L(U(t_n))$ is the spatial location of the object, and $A(U(t_n))$ is the spatial posture of the object.

3.4 Geometric change extent quantification

For different types, we choose different quantification methods to quantify the change scale (Table 2), where $D(x)$ is the change in the object, $L(t_n)$ is the spatial position, $V(t_n)$ is the spatially occupied volumes, $A(t_n)$ is the spatial attitude, and $S(t_n)$ is the length, width, or height of the object.

Change type	Quantitative method	Mathematical description
appeared	Position and volume	$D(x) = (L(t\quad), V(t\quad))$
disappeared	Position and volume	$D(x) = (L(t_n), V(t_n))$
reduced	Length change	$D(x) = S(t\quad) - S(t_n)$
grew	Length change	$D(x) = S(t_n) - S(t\quad)$
moved	Position change	$D(x) = f(L(t\quad), L(t_n))$
rotated	Posture change	$D(x) = f(A(t\quad), A(t_n))$

Table 2. Quantification of change scales.

3.4.1. Length and volume change: The four types of changes: appeared, disappeared, reduced and grew, can be quantified by calculating the length and volume of buildings that have grown or been demolished.

The length change can be calculated by:

$$\Delta L = H_2 - H_1, \tag{6}$$

where ΔL is the change length, H_1 is the building height in the first period of point cloud, and H_2 is the building height in the second period of point cloud.

The volume change can be calculated by:

$$\Delta V = V_2 - V_1, \tag{7}$$

or:

$$\Delta V = l \cdot m \cdot h, \tag{8}$$

where ΔV is the volume change, V_1 is the building volume in the first period of point cloud, and V_2 is the building volume in the second period of point cloud, l, m, h are the changes in the length, width, and

height of building.

3.4.2 Posture change: Due to data density and structural occlusion, there may be some missing components. Still, the collected point cloud of construction components is a proper subset of the real model of construction components. The surface features will not be completely lost, so in this case, the normal vector distribution features can also be used to complete the point cloud alignment.

Gaussian mapping of normal vectors. Taking the center of the externally connected sphere of the object as the computational center, the normal vectors $\overrightarrow{N_i}(\overrightarrow{N_{xi}}, \overrightarrow{N_{yi}}, \overrightarrow{N_{zi}})$ are computed at each point of the point cloud. All the normal vectors are projected onto the Gaussian sphere. The normal vector starting point falls on the center $O(0,0,0)$ of the Gaussian sphere, and the endpoint falls on the Gaussian sphere surface; the radius of the Gaussian sphere is r. Then, the Gaussian mapping point cloud $P_i(x_i, y_i, z_i)$ of the construction element:

$$\begin{cases} x_i = r \cdot \overrightarrow{N_{xi}} \\ y_i = r \cdot \overrightarrow{N_{yi}} \\ z_i = r \cdot \overrightarrow{N_{zi}} \end{cases} \quad (9)$$

Gaussian mapping point cloud clustering. We perform K-means clustering (Saglam et al., 2020) on the Gaussian-mapped point cloud of construction elements to extract the cluster centers (Fig. 3(b)). The clustering center serves as the densest point of the normal direction distribution, which we use as the feature point for Gaussian sphere alignment. At the same time, we obtain clusters with consistent normal direction (Fig. 3(a)), which are described specifically in Section *III.D.c.*

Solving for posture change. We compute the rotation matrix using the clustering center of the Gaussian-mapped point cloud as the feature point.

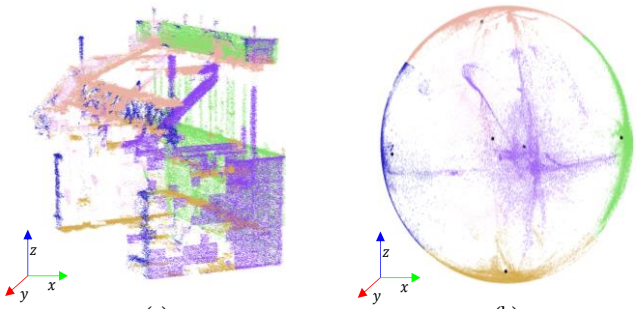

(a) (b)

Figure 3. Gaussian mapping and mean clustering isotropic plane extraction. (a) Gaussian sphere clustering corresponding to component point clouds (b) Gaussian mapping point cloud clustering (black point cloud is the center of clustering).

Extract the clustering centers of each point cloud cluster in the two objects A, B respectively and obtain the point sets M_k, N_k. Correspond the points in the point sets M_k and N_k two by two randomly to obtain k groups of point pairs, calculate the angular distances θ_k from each pair of points to the origin O, and calculate the sum of angular distances of the k groups of pairs E_k.

$$\theta_k = arccos \frac{r^2 - [(x_m - x_n)^2 + (y_m - y_n)^2 + (z_m - z_n)^2]}{2r^2}, \quad (10)$$

$$E_k = \sum_{k=0}^{k} \theta_k, \quad (11)$$

where r is the radius of the Gaussian sphere, x_m, y_m, z_m and x_n, y_n, z_n are the coordinates of the corresponding points in the M_k, N_k point sets.

The sum of angular distances for all combinations E_k is calculated iteratively, and the homonymous point correspondences of the two construction component point sets M_k and N_k are determined when E_k is smallest.

Four pairs of homonymous clustering center points are arbitrarily selected to solve the Gaussian sphere rotation matrix R using the SVD (singular value decomposition) method (Arun et al., 1987), and the rotation matrix of the Gaussian sphere S_B to S_A is the rotation matrix R of component B to A:

$$R = \begin{pmatrix} r & r_{12} & r_{13} \\ r_2 & r_{22} & r_{23} \\ r_3 & r_{32} & r_{33} \end{pmatrix}. \quad (12)$$

3.4.3. Position change: When Gaussian mapping point cloud clustering in Section III.D.b, we separate the clusters with the same normal direction, and each cluster is all the planes in that normal direction. According to the summation principle of space vector decomposition, the sum of the projections of the distances of two elements in any three directions on the coordinate axes can be calculated to obtain the spatial position change distance of elements.

Determine the main plane of the element. Priority is given to selecting the three direction point cloud clusters with the most uniform distribution of the normal direction in the element. The largest area and the densest point cloud in each point cloud cluster is extracted as the main plane in that direction, by the regional growth clustering method. Such as Fig. 4(b) for the clusters of planes with the same direction, in which the red point cloud is the main plane.

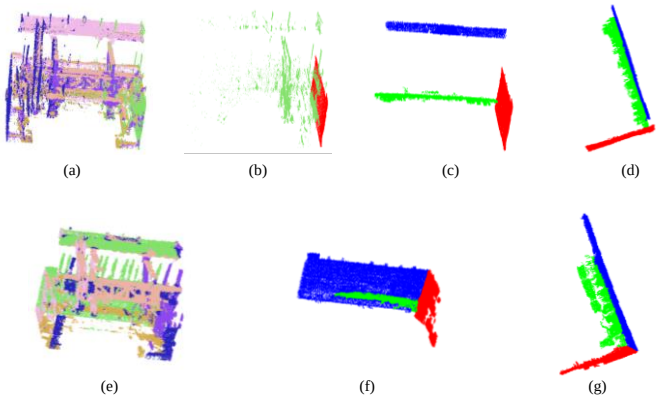

(a) (b) (c) (d)

(e) (f) (g)

Figure 4. Extraction of three pairs of principal planes of counterpart elements. (a)(e) Two counterpart elements (b) principal planes in a certain direction (c)(f) three pairs of principal planes corresponding to the direction (d)(g) top view of three pairs of principal planes.

Similarly, as Fig. 4 extracts the three pairs of isotropic principal planes of the corresponding elements, if there are problems such as uneven distribution of the normal direction of the largest principal plane, other planes can be selected to replace (Fig. 4(c)), but it is necessary to ensure that the replacement plane and the original plane have zero distance in that direction.

Solving for position change. The distance of the three pairs of principal planes is calculated and projected to the coordinate axes. The sum of the distances in the direction of each axis is found, for attaining the moving distance of the element in the direction of each axis. Corresponding to the calculation of the distance from the principal planes as shown in Fig. 5.

This contribution has been peer-reviewed. The double-blind peer-review was conducted on the basis of the full paper.
https://doi.org/10.5194/isprs-annals-X-4-2024-125-2024 | © Author(s) 2024. CC BY 4.0 License.

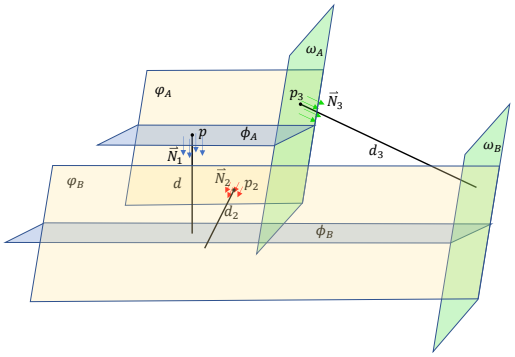

Figure 5. Main plane distance calculation.

Take the plane (φ_A, φ_B) as an example, the distance from the plane φ_B to the plane φ_A is the distance from the centroid p_1 of the plane φ_A to the plane φ_B, and the plane φ_B is in the same direction as the normal direction of φ_A, which is written as $(n_{\varphi x}, n_{\varphi y}, n_{\varphi z})$, and the translation matrix T of component B' to A is:

$$T = \begin{vmatrix} n_{\varphi x} \cdot d_1 + n_{\phi x} \cdot d_2 + n_{\omega x} \cdot d_3 \\ n_{\varphi y} \cdot d_1 + n_{\phi y} \cdot d_2 + n_{\omega y} \cdot d_3 \\ n_{\varphi z} \cdot d_1 + n_{\phi z} \cdot d_2 + n_{\omega z} \cdot d_3 \end{vmatrix}, \quad (13)$$

where $(n_{\varphi x}, n_{\varphi y}, n_{\varphi z}), (n_{\phi x}, n_{\phi y}, n_{\phi z})$, and $(n_{\omega x}, n_{\omega y}, n_{\omega z})$ are the normal directions of the planes $\varphi_A, \phi_A, \omega_A$ respectively, and d_1, d_2, and d_3 are the distances between the planes φ_A and φ_B, planes ϕ_A and ϕ_B, and the planes ω_A and $\omega_B$respectively.

4. Experiment and analysis

4.1 Experimental data

Scene 1 is a suspension bridge construction site. We collected two periods of laser point cloud data in June 2022 and May 2023; due to the equipment, data from May 2023 have no true color data. The scene range is approximately 500 m×280 m, the bridge construction adopts the longitudinal segmental pouring method, and the construction was carried out at a single point from bottom to top. The construction scene has a wide range, but the changing area is centrally distributed, and there are a lot of non-artificial object changes and data noise interference.

Scene 2 is a construction site for a high-speed rail simple supported girder bridge, and we use four periods of time series laser point cloud data collected in April 2022, June 2022, January 2023, and July 2023 for the experiments, with a scene range of approximately 510 m × 100 m. The construction of the bridge adopts a hanging basket to assist in the prefabricated component assembly method, and the construction is advanced from different abutments to the sides. The construction scene is distributed in a band, with scattered change areas, wide periods, complex change types, and some non-artificial objects change interference and data noise interference.

Before conducting the experiment, we manually observed the changes in the construction scenes and used them as the true values to verify the findings of this study by comparing them with these true values. There are 7 change objects in Scene 1, including 4 types of changes as shown in Fig. 6. In Scene 2, the changes are different in different periods, mainly concentrated in the piers, bridge bodies, cranes, tower cranes, and hanging baskets, including 5 semantic changes. In order to clearly observe the multi-temporal changes on the construction site, we select a group of sites to display as shown in Fig. 7.

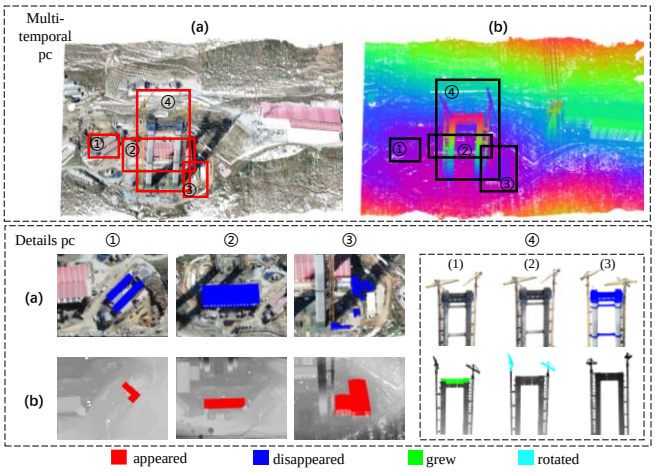

Figure 6. Scene 1: Comparison of the two periods at the construction site. (a) Period-1 point cloud, (b) Period-2 point cloud. Among them, ①–④ are local detailed images: ①–③ are buildings disappeared and new buildings appeared at the original site, ④ is the changes of bridges. (1) is the grew of bridges, (2) is the rotated tower cranes, and (3) is the disappearance of construction elements.

4.2. Experimental results and evaluation

4.2.1 Change objects extraction: The change objects in the scene are extracted using the clustering method, and the final geometric change detection results are shown in Fig. 8, which can accurately detect all the man-made objects in the scene. In Scene 1, there are 7 changes in man-made objects, which can be extracted accurately and completely, and the two factory buildings in the lower right corner of the scene are similar to each other, which can also be distinguished and extracted.

In Scene 2, the changes for different periods can be extracted completely as shown in Fig. 8. However, because the hanging basket and the bridge are nested distributed, the clustering algorithm cannot segment them correctly, and they need to be separated manually in the later stage of the study.

4.2.2 Semantic change process description: Extracting change objects are not sufficient to elaborate changes in the construction site. In order to continuously track the state of the change objects, the site needs to be analyzed in conjunction with the change semantics of the change objects.

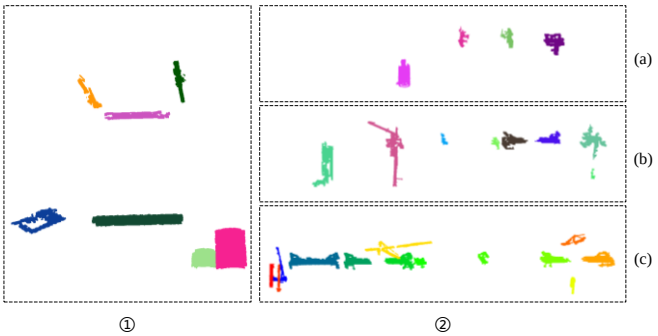

Figure 8. The results of two scenes change detection experiment. Scene 1 man-made objects change results are shown in ① while ② displays Scene 2 man-made objects change results. The latter includes point cloud change results for the 02 Period-01 Period, 03 Period-02 Period, and 04 Period-03 Period, denoted by (a–c).

We experimentally determined the change type for each object in the scenes (Fig. 9, Fig. 10), which allows us to accurately determine the object change type to monitor the situation in the construction project and observe the construction area. In Scene 1 shown in Fig. 9, during the observing period, the stage construction of the suspension bridge abutments was completed. The auxiliary construction steel frames were removed and dismantled two plants, by constructing a new plant in an area with more frequent construction activities according to the need for personnel housing was reduced.

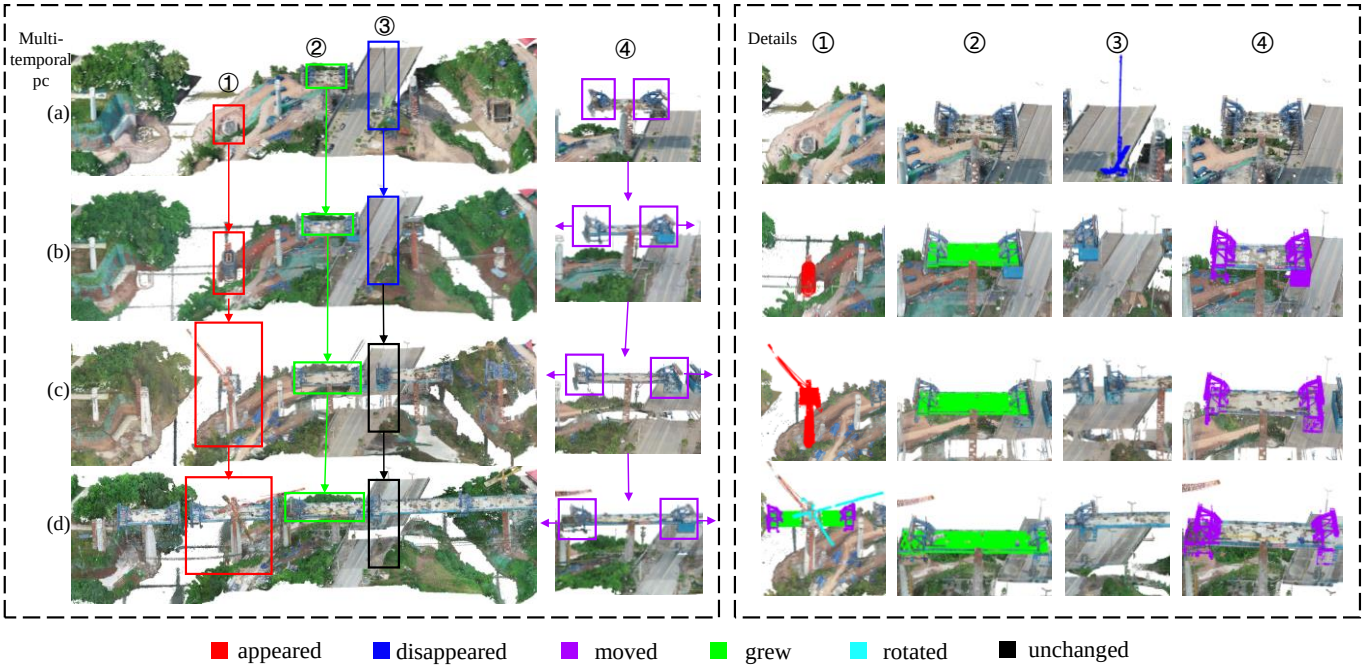

Figure 7. Scene 2: Comparison of construction site point clouds in four periods. (a)–(d) are the time-series point clouds of Periods 01, 02, 03, and 04. The different states of regions ①–④ in the four periods (identified by boxes and arrows connecting them, and the change type is identified by the colors). ① is a new pier grew in the period (a–c), and the bridge grew, the hanging baskets moved and the tower cranes rotated in the period (c–d); ② is the bridge grew in the period (a–d); and ③ is the cranes disappeared in the in the period (a–b) and no change in the period (b-d); ④ is the hanging baskets moved towards both ends.

In Scene 2 as shown in Fig. 10, during the construction period, work was carried out on the bridge, focusing on the main road and extending it to both sides. The construction involved building piers by casting a steel frame structure, with priority given to repairing the piers before mending the bridge body. Both tasks were synchronized to ensure a smooth workflow. The construction proceeded methodically, but the pace and timing of completion remain uncertain. Accurate tracking of construction progress necessitates further quantification of the scope and scale of changes.

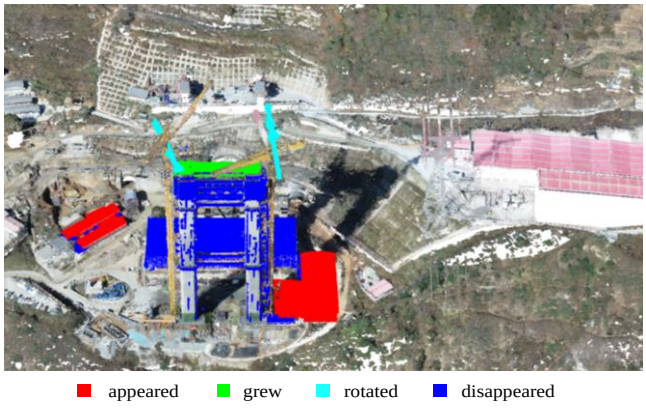

Figure 9. Analysis of change types in the construction scenes of suspension bridges (change types are identified by colors).

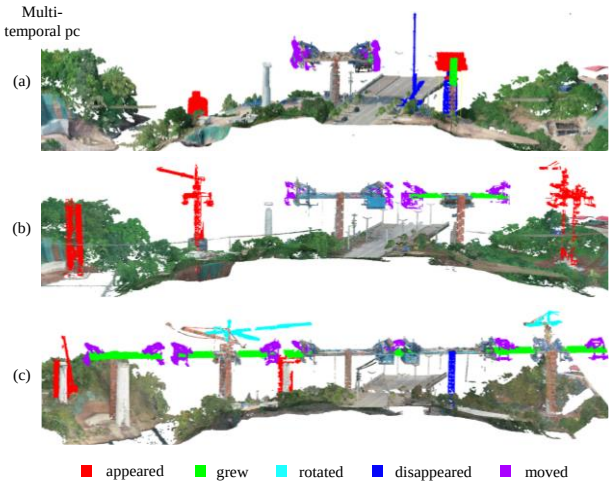

Figure 10. Illustrates the analysis of changes in construction scenes for simply supported girder bridges. (a–c) Point cloud variations of Period-02 versus Period-01, Period-03 versus Period-02, and Period-04 versus Period-03.

4.3 Geometric change extent quantization

Knowing the semantics of the changes in the construction site is

not enough to fully grasp the progress of construction, only through the precise quantification of numerical indicators to monitor the progress accurately.

As shown in Fig. 11, in Scene 1, from June 2022 to May 2023, there were two new plants (a) built at the suspension bridge construction site, with an area of 9919.75 m^3 and 3522.38 m^3 respectively. Two plants (b) with an area of 2248.74 m^3 and 1533.54 m^3 were dismantled. The volume of the dismantled plant (c) was 46023.51 m^3 smaller than that of the original. In addition to testing the site environment, the construction progress can also be monitored. The construction of the cable tower (d) completed its construction phase, the steel frame was removed, and the cable tower grew by 5.18 m compared with the previous period.

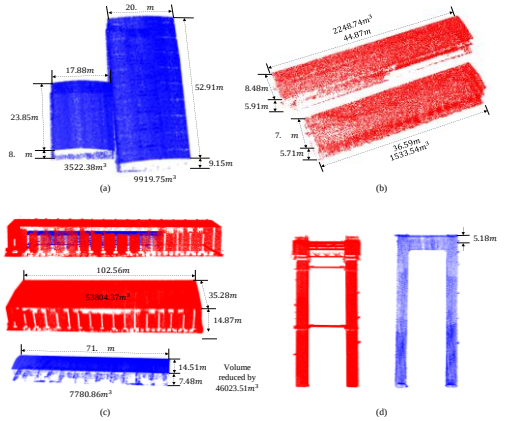

Figure 11. Quantitative analysis of change. (a) appeared (b) disappeared (c) disappeared and appeared (d) grew.

In Scene 2, according to the analysis of temporal changes in the site (see in Fig. 12), the foundation of bridge pier (b) was constructed, and the heights rose by 17.75 m, 11.89 m, and 4.85 m during the observation period. The bridge body (c) was continuously constructed to both sides; the left sides of the bridge body were built into 3.46 m, 4.37 m, and 9.53 m, and the right sides of the bridge body were built into 3.35 m, 3.62 m, 6.62 m. Construction equipment (d) was on site in April 2022 and disappeared in the next period. Roughly quantifying the positional changes in the two hanging baskets(a), the left basket advanced by 3.16 m, 4.44 m, and 4.18 m during the observation period, and the right basket advanced by 3.58 m, 3.79 m, and 5.94 m. Upon careful observation, there were subtle changes in the posture of the hanging baskets, so we calculated the specific posture and position changes as shown in Table 3.

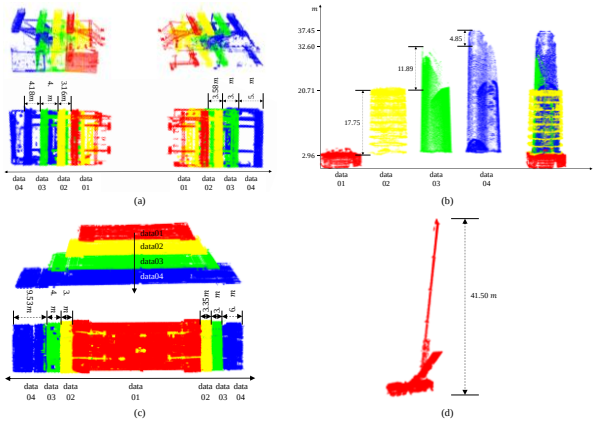

Figure 12. Quantitative analysis of different changes (1). (a) Cradle moved, (b) Abutment grew, (c) bridge grew, (d) Crane disappeared

	Posture changes			Positional changes		
Left cradle	Yaw	pitch	roll	x-axis	y-axis	z-axis
02-01	1.78	4.47	−0.63	−2.44	−3.53	6.24
03-02	−2.01	−2.87	−5.40	−4.90	0.77	−0.51
04-03	−0.29	−3.84	−1.95	−3.43	−1.08	−4.16
Right cradle						
02-01	−2.29	0.17	0.92	1.68	5.54	−0.37
03-02	0.00	0.34	−0.34	3.66	1.30	0.98
04-03	−0.06	−0.40	0.23	5.56	2.19	−0.82

Table 3. Changes in attitude and position of the cradle.

Overall, this Section delivers a thorough account of our accomplishments. It covers man-made change objects extracting, semantic analysis of the change process, and precise geometric change calculating on the time-series point cloud data collected from the construction site. The section explains the dynamic changes within the construction area by conducting on-site observations. This allows for precise monitoring of construction progress and quality, as well as the inspection of safety hazards and potential risks at the construction site, which ultimately enhances automation in the dynamic monitoring of construction.

5. Conclusion

This study designs a change detection framework that detects object changes at construction sites using octree change detection. The approach comprises three primary parts. The first part entails accurately and robustly determining man-made change objects. The second part defines the semantics of the change process for the changed objects and considers the potential changes that may occur at construction sites. The third section entails a quantitative calculation of the extent of geometric change.

Two construction scenes are investigated, in which factors such as noise and natural change are eliminated, detection is focused on artificial objects. In our change detection workflow, the change process semantics and geometric change extent is considered in addition to extracting change objects. We present a registration approach designed for artificial objects that quickly recuperates object poses and thoroughly describes scene changes. However, as previously stated, manual observation remains necessary for the semantic labeling of altered objects. Implementing target detection can be an avenue to attain complete automation and explore immediate change detection on identical objects. This direction points to future research.

Acknowledgements

This work was supported in part by the National Key Research and Development Program of China (Project No. 2022YFF0904401) and the Natural Science Foundation of China (project numbers 42230102, 42071437), the Sichuan Science and Technology Fund for Distinguished Young Scholars 22JCQN0110.

References

Arun, KS., 19877 Least-Squares Fitting of Two 3-D Point Sets. Pattern Analysis and Machine Intelligence, *IEEE Transactions on, PAMI-9*(5):698-700.

de Gélis, I., Lefèvre, S. & Corpetti, T., 2023. Siamese KPConv: 3D multiple change detection from raw point clouds using deep learning. *ISPRS Journal of Photogrammetry and Remote Sensing*, Vol. 197, March, pp 274–291.

Du, S., Zhang, Y., Yang, Z., Zou, Z., Tang, Y., Fan, C. & Qin, R., 2016. Building change detection using old aerial images and new LiDAR data. *Remote Sensing*, 2016, 8(12), 1030.

Duong, N. D., Soladie, C., Kacete, A., Richard, P. Y., & Jérme Royan., 2019. Efficient multi-output scene coordinate prediction for fast and accurate camera relocalization from a single rgb image. *Computer Vision and Image Understanding*, 10/31, 190.

Gehrung, J., Hebel, M., Arens, M. & Stilla, U., 2018. A voxel-based metadata structure for change detection in point clouds of large-scale urban areas. *ISPRS Annals of the Photogrammetry, Remote Sensing and Spatial Information Sciences*, 4(2):97–104.

Girardeau-Montaut, D., Rouxa, M., Marcb, R & Thibault, G., 2005. Change detection on points cloud data acquired with a ground laser scanner, *International Archives of Photogrammetry, Remote Sensing and Spatial Information Sciences*, 36(3): W19.

Hebel, M., Arens, M. & Stilla, U., 2013. Change detection in urban areas by object-based analysis and on-the-fly comparison of multi-view ALS data. *ISPRS Journal of Photogrammetry and Remote Sensing*, Vol.86, Dec., pp 52–64.

Ku, T., Galanakis, S., Boom, B., Veltkamp, R.C., Bangera, D., Gangisetty, S., Stagakis, N., Arvanitis, G. & Moustakas, K.,2021. SHREC 2021: 3D point cloud change detection for street scenes. *Computers and Graphics* (Pergamon), pp 192–200.

Lague, D., Brodu, N. & Leroux, J., 2013. Accurate 3D comparison of complex topography with terrestrial laser scanner: Application to the Rangitikei canyon (N-Z). *ISPRS Journal of Photogrammetry and Remote Sensing*, Vol.82, August, pp 10–26.

Landrieu, L., & Simonovsky, M. 2018. Large-Scale Point Cloud Semantic Segmentation with Superpoint Graphs. *Computer Vision and Pattern Recognition IEEE*, pp 4558–4567.

Li, J., 2020. High-precision detection method for large and complex steel structures based on global registration algorithm and automatic point cloud generation. *Measurement*, Dec., 172.

Levine, N. M., Narazaki, Y., & Spencer, B. F., 2023. Development of a building information model-guided post-earthquake building inspection framework using 3D synthetic environments. *Earthquake Engineering and Engineering Vibration*, 22(02):279-307.

Lu, B., Wang, Q. & Li, A'N., 2019. Massive Point Cloud Space Management Method Based on Octree-Like Encoding. *ARABIAN Journal for Science and Engineering*,44(11),9397-9411.

Mntyl, M., 1986. Boolean Operations of 2-Manifolds through Vertex Neighborhood Classification. *ACM Transactions on Graphics*, 5(1):1-29.

Pagac, D., Nebot, E.M. & Durrant-Whyte, H., 1998. An evidential approach to map-building for autonomous vehicles. *IEEE Transactions on Robotics and Automation, Robotics and Automation*, pp 623–629.

Park, S. Ju, S. & Yoon, S., 2021. An efficient data structure approach for BIM-to-point-cloud change detection using modifiable nested octree. *Automation in Construction*, 132(9):103922.

Saglam, A., Makineci, H. B., Baykan, O. K., & Baykan, N. A., 2020. Clustering-Based Plane Refitting of Non-planar Patches for Voxel-Based 3D Point Cloud Segmentation Using K-Means Clustering. *Traitement du Signal: signal image parole*, (6):37.

Singh, S. K., Banerjee, B. P., & Raval, S., 2023. A review of laser scanning for geological and geotechnical applications in underground mining. *International Journal of Mining Science and Technology*,33(02):133-154.

Stilla, U., & Xu, Y., 2023. Change detection of urban objects using 3D point clouds: A review. *ISPRS Journal of Photogrammetry and Remote Sensing*, Apr., pp 228–255.

Tran, T.H.G., Ressl, C. & Pfeifer, N., 2018. Integrated Change Detection and Classification in Urban Areas Based on Airborne Laser Scanning Point Clouds. *Sensors* (Basel, Switzerland), 2018, 18(2), 448;

Wang, S., Suo, S., Ma, W.-C., Pokrovsky, A. & Urtasun, R., 2018. Deep Parametric Continuous Convolutional Neural Networks. *Computer Vision and Pattern Recognition*, pp 2589–2597.

Xiao, J. Adler, B. & Zhang, H., 2012. 3D point cloud registration based on planar surfaces. *Transactions of the Chinese Society for Agricultural Machinery*.

Xiao, W., Xu, S., Elberink, S. O., & Vosselman, G., 2016. Individual tree crown modeling and change detection from airborne lidar data. *IEEE Journal of Selected Topics in Applied Earth Observations and Remote Sensing*, 9(8):3467–3477.

Zhang, Z., Vosselman, G., Persello, C., Yang, M.Y., Gerke, M. & Tuia, D., 2019. Detecting building changes between airborne laser scanning and photogrammetric data. *Remote Sensing*, 11(20), 2417-.